Applied Physics B (2020) 126:31
https://doi.org/10.1007/s00340-019-7374-x

**Applied Physics B**
**Lasers and Optics**

# Measurements and analysis of diode laser modulation wavelength at high accuracy and response rate

**Bo Tao[1] · Qingchun Lei[2] · Jingfeng Ye[1] · Zhenrong Zhang[1] · Zhiyun Hu[1] · Wei Fan[2]**

Received: 10 April 2019 / Accepted: 28 December 2019 / Published online: 1 February 2020


## Abstract

It is a key procedure of measuring the diode laser wavelength in the wavelength modulation spectroscopy (WMS) technique since it determines the selection of specific modulation amplitude and frequency and thus the overall accuracy of the WMS technique. However, the wavelength modulation frequency of lasers is usually from tens of kHz to hundreds of kHz, which makes the traditional methods difficult to measure the wavelength with the sufficient accuracy and time response rate. Therefore, in this paper, we developed a method to measure the modulated wavelength with improved accuracy and time response rate by using a customized long fiber ring etalon. In the method, the free spectral range (FSR) of the etalon was determined by using two adjacent absorption lines of water. And the amplitude of the laser wavelength and its phase relative to the driving voltage were determined by means of interference peak identification and sinusoidal fitting. Finally, we used the developed method to measure dynamic wavelengths as well as phases of a distribute feedback (DFB) diode laser with the modulation frequency from 1 to 500 kHz and the modulation voltage from 0.2 to 1 V. Based on the measurements, the response characteristics of both the linear and nonlinear wavelengths as well as phases with modulation frequency and amplitude were obtained, which provide necessary data for the application of quantitative and high-repetition WMS technique in combustion diagnostics.

## 1 Introduction

Tunable diode laser (TDL) absorption-based sensors have been extensively studied as methods for non-intrusive measurements of gas properties in combustion due to their robust, compact, low-cost nature [1–5]. Wavelength modulation spectroscopy (WMS) is a derivative form of the absorption spectroscopy that has been increasingly applied for measurements in harsh environments in virtue of its improved sensitivity and noise-rejection capabilities [6–8]. In WMS technique, the output wavelength of the TDL is modulated at a specific frequency (i.e., from kHz to MHz), so that the corresponding absorption information is shifted to high frequencies, which facilitates the identification and detection of absorption signals by get rid of various common noise sources [6–8]. Therefore, the response of output wavelength of the TDL to modulation voltage becomes a key parameter, which determines the selection of specific modulation voltage amplitude and frequency. Furthermore, quantitative measurements of the WMS technique require accurate knowledge of laser wavelength modulation parameters (i.e., the amplitude of the laser wavelength and its phase relative to the driving voltage) [9–12].

This work was supported by the National Natural Science Foundation of China under Grant Nos. 91541203, 91641112 and 91441201, and the Foundation Project of State Key Laboratory of Laser Interaction with Matter under Grant No. SKLLIM1609.

✉ Zhiyun Hu
huzhiyun@nint.ac.cn

✉ Wei Fan
weifan419@nwpu.edu.cn

Bo Tao
taobo@nint.ac.cn

Qingchun Lei
lqc@nwpu.edu.cn

Jingfeng Ye
yejingfeng@nint.ac.cn

Zhenrong Zhang
zhangzhenrong@nint.ac.cn

[1] State Key Laboratory of Laser Interaction with Matter, Northwest Institute of Nuclear Technology, Xi'an, Shannxi, People's Republic of China

[2] School of Power and Energy, Northwestern Polytechnical University, Xi'an, Shannxi, People's Republic of China

Extensive theoretical analysis of the modulation properties of TDLs haves reported over many years [13–17]. And a relatively accurate theoretical model for the magnitude and phase of the wavelength as a function of the modulation frequency has been established. However, the theoretical model is based on approximate conditions, and the various parameters in the model depend on the specific TDLs [18]. Thus, it is necessary to measure the modulation properties of TDLs. This is due to the different TDLs, their response characteristics are different [18]. For WMS applications, the wavelength modulation amplitude of diode laser depends on the specific absorption line width, usually around 0.1 $cm^{-1}$ in an atmospheric pressure environment [9, 12]. And the wavelength modulation frequency depends on the specific measurement repetition, which is usually hundreds kHz for kilohertz-repetition-rate combustion measurements [7–9, 11]. Therefore, there is a need for the accuracy of wavelength measurement system to reach at least 0.01 $cm^{-1}$ and the response rate to reach at least megahertz to yield a high-accuracy measurement of the dynamic wavelength. To date, the commercial wavelength measuring devices cannot meet the above requirements in terms of measurement accuracy and time response rate. For example, the time response rate of the latest wavelength meters is usually around several kHz [19, 20].

To address the above issues, several types of customized wavelength measurement methods, mostly based on interferometry principles, have been developed to measure and analyze the dynamic wavelength characteristics of diode lasers. For example, Liu et al. [21, 22] measured the wavelength scanning characteristics of DFB (Distribute Feedback) diode lasers using an all-fiber Mach–Zehnder interferometer. Lytkine et al. [23] used Fabry–Perot etalon to measure the dynamic wavelength of a vertical cavity surface emitting diode laser (VCSEL) under 100 Hz sawtooth scanning. However, those methods only realized the dynamic wavelength measurement under the condition of scanning wavelength of the TDLs, not the modulation wavelength. Because measuring the modulation wavelength of TDLs is more difficult than the scanning wavelength due to the small wavelength modulation amplitude (~0.1 $cm^{-1}$) and the high wavelength modulation frequency (~100 kHz).

To measure and analyze the modulation characteristics of TDLs, the previous research works mainly used the change in the spectrum of the harmonic signal in WMS to infer the frequency response characteristics of laser wavelength with the modulation frequency [24–27]. This method was applied to measure the magnitude and phase lag of the wavelength modulation as a function of the modulation frequency for several specific lasers including a 2 μm DFB laser [24], 0.763–2.3 μm VCSELs [25, 26] and a 3 μm interband cascade laser [27]. However, this method is based on the assumption that the laser wavelength changes linearly with the injection current and thus only linear wavelength modulation parameters can be measured. In practice, however, the wavelength of the diode laser varies nonlinearly with the injection current, especially at large current modulation amplitude, which is demonstrated in this paper.

In this paper, we developed a method to measure the modulated wavelength with improved accuracy and time response rate using a customized long fiber ring etalon and a high-speed data acquisition card. In the proposed method, the free spectral range (FSR) of the etalon was determined using two adjacent absorption lines of water. And the amplitude of the laser wavelength and its phase relative to the driving voltage was determined by means of interference peak identification and sinusoidal fitting. Based on the developed method, we measured the dynamic modulation wavelength of DFB diode lasers at the modulation frequency from 1 to 500 kHz and the modulation voltage from 0.2 to 1 V which corresponds to a modulation current from 4 to 20 mA. The wavelength measuring accuracy can be better than 0.0005 $cm^{-1}$ and the time response rate can be better than 25 MHz.

## 2 Description of the method

The wavelength modulation mechanism of DFB laser is due to the change of equivalent refractive index in the resonant cavity when the injection current of the laser changes [18]. In practice, the injection current of the DFB laser can be adjusted by the driving voltage of the laser controller. The driving voltage ($U$) of the diode laser can be written as:

$$U(t) = u \cdot \sin(2\pi ft) \tag{1}$$

Then the varying wavelength ($cm^{-1}$) of the laser can be expressed as:

$$\Delta\nu = a_1 \cdot \sin\left(2\pi ft + \varphi_1\right) + a_2 \cdot \sin\left(4\pi ft + \varphi_2\right) \tag{2}$$

where $u$ is the modulation amplitude (V), $f$ is the modulation frequency (Hz); $a_1$ and $a_2$ are linear modulation depth and nonlinear modulation depth ($cm^{-1}$) of wavelength, respectively; $\varphi_1$ and $\varphi_2$ are the corresponding phase shifts (rad) with respect to the driving voltage. Thus, for a specific drive voltage, the dynamic parameters of wavelength to be measured are $a_1$, $\varphi_1$, $a_2$, $\varphi_2$.

Figure 1 shows the schematic setup of the dynamic wavelength and phase measurement system. The DFB laser used here is a fiber-coupled laser (NTT Electronics, NLK1E5EAAA) emitting wavelength near to 1.4 μm. An ILX Lightwave LDC-3724 is used to control the laser temperature and current. A function generator (Tektronix, AFG310) is used to modulate the injection current and thus the wavelength of laser. The current–voltage ratio is

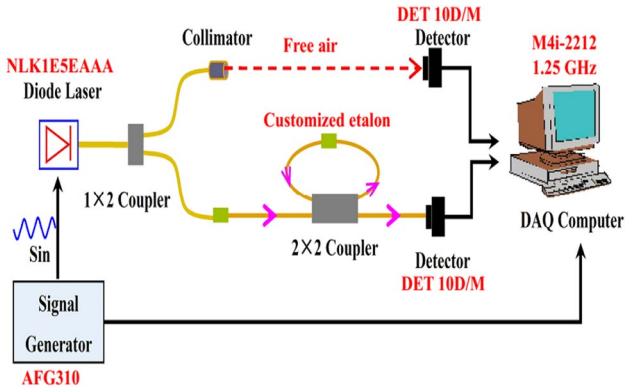


**Fig. 1** Schematic setup of the dynamic wavelength and phase measurement system

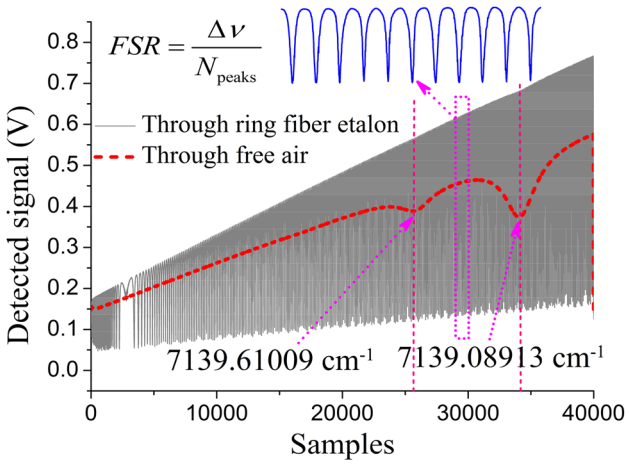


**Fig. 2** Laser intensity in the measurement of free spectral range of the ring fiber etalon

20 mA/V for LDC-3724 laser controller. A 1 × 2 fiber coupler is used to split the laser into two beams. One beam passes through the free air in order to monitor the change of laser intensity. The other beam passes through a ring fiber etalon, which is customized using a 2 × 2 optical fiber coupler and has a cavity structure with a length of 120 cm. Two high speed detectors (Thorlabs, DET 10D/M) are utilized to detect the transmitted laser signals. The detected signals are recorded by a data acquisition system with a sampling rate of 1.25 GHz (Spectrum, M4i-2212). The data acquisition system also synchronously collects the driving voltage signal so as to obtain the phase information of the driving voltage.

The free spectral range (FSR) of the ring cavity etalon can be calculated by FSR = $c/nl$, where $c$ is the speed of light in vacuum, $n$ is the refractive index of the medium in the optical cavity, and $l$ is the length of the optical cavity. However, the length of cavity $l$ and the refractive index $n$ vary with different materials and temperatures, and it is not easy to get accurate values. Instead, this work uses two adjacent absorption lines of water (i.e., 7139.61009 $cm^{-1}$ and 7139.08913 $cm^{-1}$) in free air to determine the FSR of the ring fiber etalon with a uncertainty of 0.00001 $cm^{-1}$. More specifically, the laser wavelength is tuned to the above selected absorption lines. The scanned laser transmitted through the free air thus exhibits two absorption depressions, whose center positions corresponds to the center wavelength of the two selected absorption lines. In contrast, the laser passing through the ring fiber etalon exhibits various interference peaks during the wavelength scanning. Figure 2 presents the typical laser intensity in the measurement of free spectral range of the ring fiber etalon. The wavelength interval between the two adjacent interference peaks is the FSR of the etalon, which is calculated to be 0.0057 $cm^{-1}$ by counting the number of interference peaks between the two absorption lines.

The information of modulation wavelength parameters (i.e., $a_1$, $\varphi_1$, $a_2$, $\varphi_2$) are hidden in the interference peaks, so there is a need to accurately identify the interference peaks. Figure 3 shows the original and filtered signals of interference peaks under sinusoidal wavelength modulation. The driving voltage of the laser is 0.5 V and the

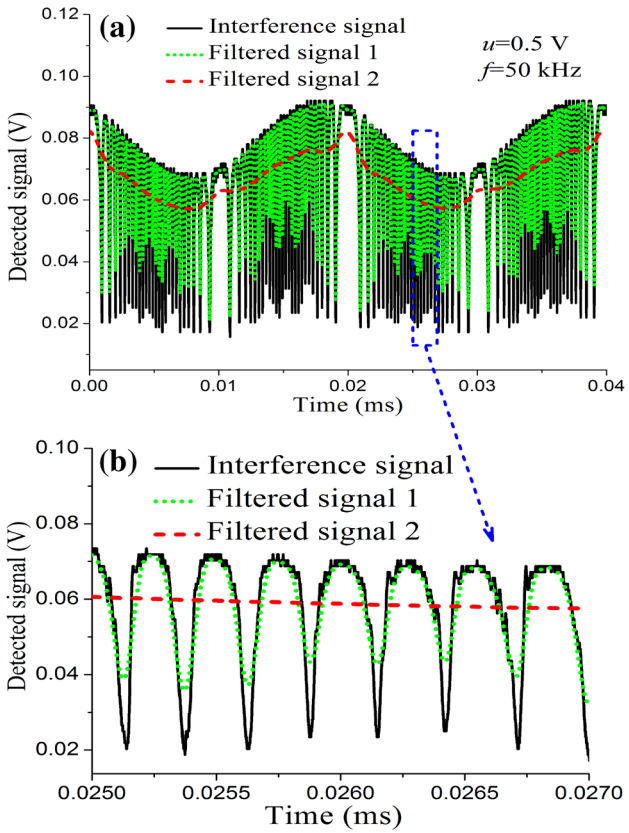


**Fig. 3** Typical interference peaks and its data processing process under sinusoidal wavelength modulation. **a** The measured interference peaks in two modulation periods. **b** The enlarged view of the blue dashed border in (**a**)

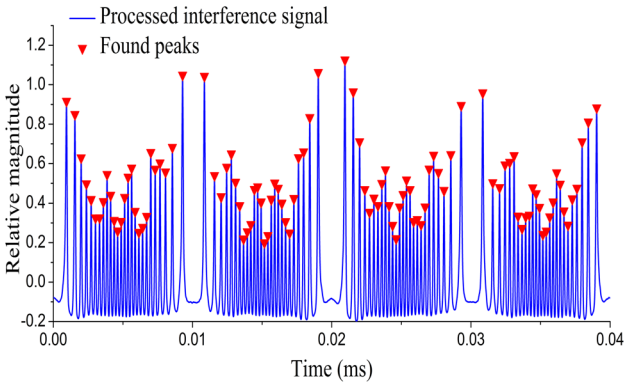


**Fig. 4** Processed interference signal and peaks identification

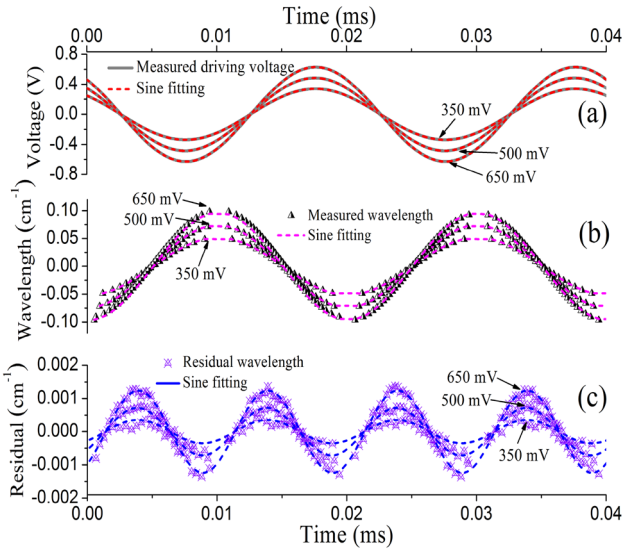


**Fig. 5** The synchronous measured driving voltage and laser wavelength as a function of time. **a** The measured driving voltage at 350 mV, 500 mV, 650 mV and their sinusoidal fitting. **b** The measured laser wavelengths and their sinusoidal fitting. **c** The residual error of (**b**) and their sinusoidal fitting at doubling frequency

frequency is 50 kHz in Fig. 3. As seen, the original interference signals are filtered twice. The first filter uses a low-order low-pass filter, the main purpose of which is to remove the burrs from the original signal and retain the interference peaks position information, as indicated by the green dotted line in Fig. 3. The second filter uses a high-order low-pass filter, which is mainly to obtain the baseline of the original interference peaks signal, as indicated by the red dashed line in Fig. 3. Based on the two filtered signals, the high signal-to-noise ratio interference peaks signal can be obtained by performing natural logarithm operation of the two filtered laser signals. The results are shown in Fig. 4. It can be seen that the processed interference signal is clean and free of burrs, and then the position of each peaks can be accurately found through the peak-to-valley identification function, as indicated in the red triangle points in Fig. 4.

The wavelength interval between the adjacent interference peaks in Fig. 4 is the free spectral range of the ring fiber etalon, which is measured to be 0.0057 cm$^{-1}$. Based on the positions of interference peaks shown in Fig. 4, the wavelength between adjacent interference peaks can be obtained. Figure 5b shows a time-dependent wavelength calculated using interference peaks position information, and then $a_1$ and $\varphi_1$ in Eq. (2) can be obtained by fitting the wavelength data with a Sine function. A further sinusoidal fitting of the residual error in Fig. 5b results in $a_2$ and $\varphi_2$ in Eq. (2), as shown in Fig. 5c. Although the free spectral range of the ring fiber etalon is 0.0057 cm$^{-1}$, $a_1$ and $a_2$ are obtained on the basis of sinusoidal fitting. It can be seen from Fig. 5c that the final wavelength measurement accuracy is better than 0.0005 cm$^{-1}$. As for the time response rate of the wavelength data, since the sampling rate of the acquisition card in the measurement system is 1.25 GS, even if a complete interference peak requires 50 data points to be recorded, the wavelength measurement rate of the developed method can reach 25 MHz.

## 3 Measurement results and analysis

Based on the measurement system and data processing procedure described in Sect. 2, the dynamic wavelength parameters ($a_1$, $\varphi_1$, $a_2$, $\varphi_2$) at different modulation amplitudes and frequencies can be acquired. Figure 6 shows the relationship of linear wavelength modulation depth $a_1$ and phase $\varphi_1$ of diode laser wavelength to driving voltage at different modulation frequencies. It can be seen that $a_1$ has a linear relationship with the driving voltage amplitude, and the slope of line varies for different modulation frequencies. For example, it decreases with the increase of modulation frequency, as shown in Fig. 6a. As for the $\varphi_1$, Fig. 6b shows that the $\varphi_1$ is almost constant at different driving voltages, but it decreases with the increase of modulation frequency.

Defining the linear wavelength modulation rate $k_1 = a_1/u$, Fig. 7 shows the measured $k_1$ and $\varphi_1$ as a function of modulation frequency. It can be seen that $k_1$ decays rapidly with the increase of modulation frequency. According to the nonlinear fitting of the measured data, it shows that $k_1$ has the second order exponential decay, rather than the simple first order exponential decay, as shown in Fig. 7a. In contrast, $\varphi_1$ decays almost linearly with the increase of modulation frequency, as shown in Fig. 7b. The basic characteristic of DFB diode laser is that the output wavelength (expressed by wavenumber) decreases with the increasing modulation voltage, so $\varphi_1 = \pi$ under ideal conditions. However, according to the measurement results shown in Fig. 7b, $\varphi_1$ only approaches to $\pi$ at very low modulation frequency and gradually deviates

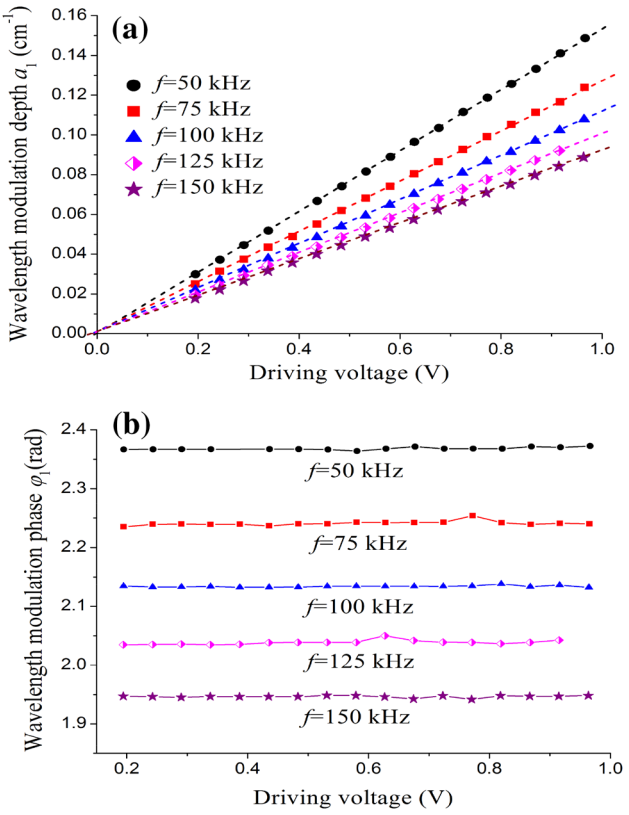


**Fig. 6** Linear wavelength modulation depth $a_1$ (**a**) and phase $\varphi_1$ (**b**) varying with driving voltage at different modulation frequencies

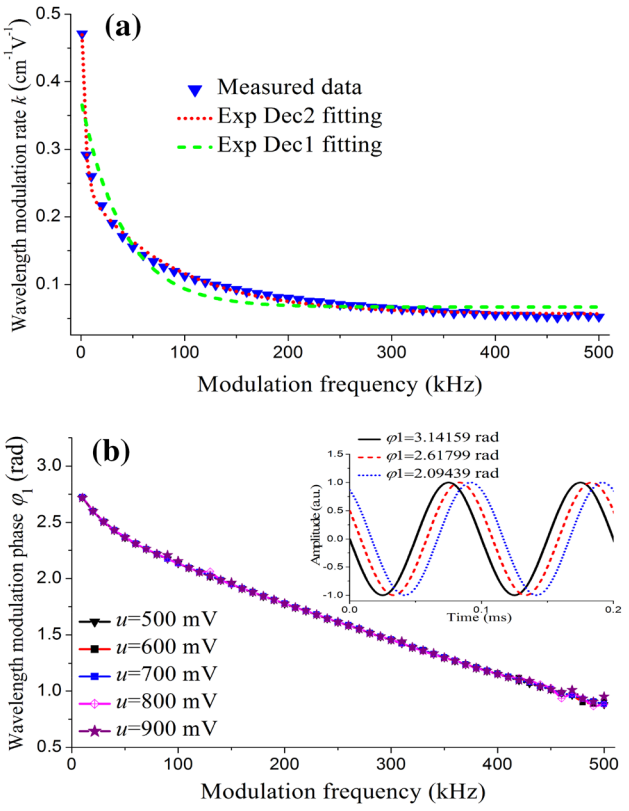


**Fig. 7** Measured linear wavelength modulation rate $k_1 = a_1/u$ (**a**) and phase $\varphi_1$ (**b**) as a function of modulation frequency

to π as the modulation frequency increases. The sub-figure in Fig. 7b shows that the phase of the response wave delays with a smaller $\varphi_1$, and the delay increases with the increase of the modulation frequency.

Figure 8 shows the relationship between measured nonlinear wavelength modulation depth $a_2$ and phase $\varphi_2$ and the modulation frequency with different driving voltages. According to Fig. 8, the following conclusions can be drawn: (1) $a_2$ increases with the increase of modulation voltage, and $a_2$ decays nonlinearly with the increase of modulation frequency; (2) similar to the $\varphi_1$, $\varphi_2$ is almost the same at different modulation voltages, but it decays linearly with the increase of modulation frequency.

In WMS applications, the ratio of $a_2$ to $a_1$ is important because this value determines the distortion of WMS spectrum caused by the nonlinear response of diode laser wavelength. Figure 9 shows $a_2/a_1$ as a function of modulation frequency and voltage. The following conclusions can be drawn from Fig. 9: (1) there is no obvious variation tendency of $a_2/a_1$ with modulation frequency, and the fluctuations shown in Fig. 9a are mainly caused by the measurement errors; (2) $a_2/a_1$ increases with the increase of modulation voltage, and the relationship between $a_2/a_1$ and modulation voltage is linear, as shown by the linear fitting in Fig. 9b.

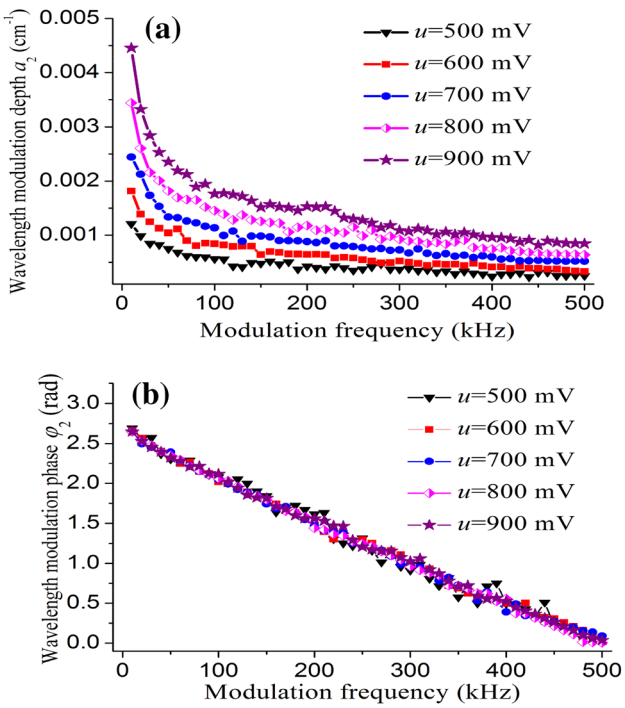


**Fig. 8** Nonlinear wavelength modulation depth $a_2$ (**a**) and phase $\varphi_2$ (**b**) varying with driving voltage at different modulation frequencies

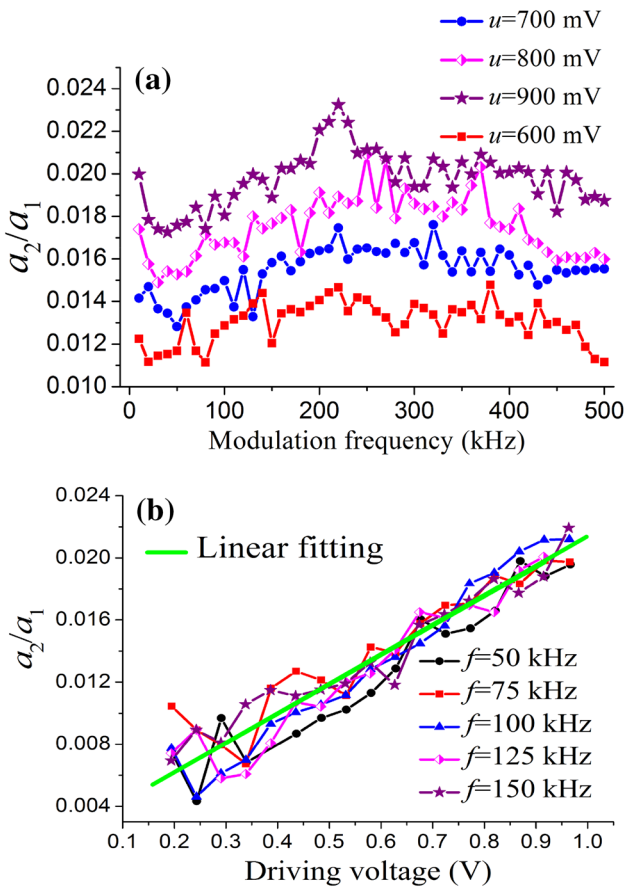


**Fig. 9** The ratio of nonlinear wavelength modulation depth $a_2$ to linear wavelength modulation depth $a_1$ varying with modulation frequency (**a**) and driving voltage (**b**)

As is known, if we want to increase the measurement repetition of WMS technique, we need to increase the wavelength scanning frequency and correspondingly the wavelength modulation frequency [9–12]. According to the measurement results in this paper, the measurement repetition of WMS technique is limited by two points: (1) the highest modulation current of diode laser, which is due to a large modulation current required for the high modulation frequency; (2) WMS spectrum distortion caused by nonlinear wavelength modulation, because the higher the modulation frequency, the greater the corresponding modulation current, resulting in the greater $a_2$.

## 4 Conclusions

This work developed a method for the measurement of modulation characteristics of DFB diode laser. The wavelength measuring accuracy can be better than 0.0005 $cm^{-1}$ and the time response rate can be better than 25 MHz. Based on the developed method, the response characteristics of both the linear and nonlinear wavelengths as well as phases with modulation frequency and amplitude were obtained. The main conclusions are as follows: (1) the linear wavelength modulation depth $a_1$ varies linearly with the modulation voltage, and the slope of line decays with the increase of modulation frequency in a second-order exponential function; (2) the linear wavelength phase $\varphi_1$ remains constant with different modulation voltages, but it decreases with the increase of modulation frequency; (3) the ratio of the nonlinear wavelength modulation depth $a_2$ to linear wavelength modulation depth $a_1$ ($a_2/a_1$) increases linearly with modulation voltage, but $a_2/a_1$ remains almost constant with different modulation frequency; (4) the variation of nonlinear wavelength phase $\varphi_2$ with modulation frequency and modulation voltage is similar to $\varphi_1$.

## References

1. C.S. Goldenstein, R.M. Spearrin, J.B. Jeffries, R.K. Hanson, Infrared laser-absorption sensing for combustion gases. Prog. Energ. Combust. **60**, 132–176 (2016)
2. M.A. Bolshov, Y.A. Kuritsyn, Y.V. Romanovskii, Tunable diode laser spectroscopy as a technique for combustion diagnostics. Spectrochim. Acta B At. Spectrosc. **106**, 45–66 (2015)
3. R.K. Hanson, D.F. Davidson, Recent advances in laser absorption and shock tube methods for studies of combustion chemistry. Prog. Energ. Combust. **44**, 103–114 (2014)
4. H. Nasim, Y. Jamil, Diode lasers: from laboratory to industry. Optics Laser Technol. **56**, 211–222 (2014)
5. W.W. Cai, C.F. Kaminski, Tomographic absorption spectroscopy for the study of gas dynamics and reactive flows. Prog. Energ. Combust. **59**, 1–31 (2016)
6. M. Matsuia, T. Yamada, High sensitive translational temperature measurement using characteristic curve of second harmonic signal in wavelength modulation spectroscopy. Rev. Sci. Instrum. **88**, 013105 (2017)
7. C.S. Goldenstein, C.L. Strand, I.A. Schultz, K. Sun, J.B. Jeffries, R.K. Hanson, Fitting of calibration-free scanned wavelength modulation spectroscopy spectra for determination of gas properties and absorption lineshapes. Appl. Opt. **53**(3), 356–367 (2014)
8. Z.C. Qu, R. Ghorbani, D. Valiev, F.M. Schmid, Calibration-free scanned wavelength modulation spectroscopy–application to $H_2O$ and temperature sensing in flames. Opt. Express **23**(12), 16492–16499 (2015)
9. B. Tao, Z.Y. Hu, W. Fan, S. Wang, J.F. Ye, Z.R. Zhang, Novel method for quantitative and real-time measurements on engine combustion at varying pressure based on the wavelength modulation spectroscopy. Opt. Express **25**(16), A762–A776 (2017)
10. Z.M. Peng, Y.J. Ding, L. Che, Q.S. Yang, Odd harmonics with wavelength modulation spectroscopy for recovering gas absorbance shape. Opt. Express **20**(11), 11976–11985 (2012)
11. R. Sur, K. Sun, J.B. Jeffries, J.G. Socha, R.K. Hanson, Scanned-wavelength-modulation-spectroscopy sensor for CO, $CO_2$, $CH_4$ and $H_2O$ in a high-pressure engineering-scale transport-reactor coal gasifies. Fuel **150**, 102–111 (2015)
12. Z.C. Qu, F.M. Schmidt, In situ $H_2O$ and temperature detection close to burning biomass pellets using calibration free wavelength modulation spectroscopy. Appl. Phys. B **119**, 45–53 (2015)
13. M. Ishikawa, R. Nagarajan, T. Fukushima, J.G. Wasserbauer, J.E. Bowers, Long wavelength high-speed semiconductor lasers

with carrier transport effects. IEEE J. Quantum Electron. **28**(10), 2230–2241 (1992)
14. J. Kinoshita, Modelling of high-speed DFB lasers considering the spatial holeburning effect using three rate equations. IEEE J. Quantum Electron. **30**(4), 929–938 (1994)
15. J.Y. Chen, R. Maciejko, T. Makino, Dynamic properties of push-pull DFB semiconductor lasers. IEEE J. Quantum Electron. **32**(12), 2156–2165 (1996)
16. X. Wang, L. Chrostowski, High-speed Q-modulation of injection-locked semiconductor laser. IEEE Photon. J. **3**(5), 936–945 (2011)
17. D. Che, F. Yuan, W. Shieh, Towards high-order modulation using complex modulation of semiconductor lasers. Opt. Express **24**(6), 6644–6649 (2016)
18. T. Benoy, M. Lengden, G. Stewart, W. Johnstone, Recovery of absorption line shapes with correcion for the wavelength modulation characteristics of DFB lasers. IEEE Photon. J. **8**(3), 1501717 (2016)
19. Bristol instruments, 871 Series Laser Wavelength Meter. https://www.bristol-inst.com/products/wavelength-meters-scientific/871-series-pulsed-laser-wavelength-meter. Accessed 1 Feb 2020
20. HighFinesse, "Sensitive and compact wavemeter with a large spectral range for high speed measurements of pulsed and continuous lasers," Available: http://www.highfinesse.com/en/wavelengthmeter/54/ws8-series
21. J.W. Liu, Z.Y. Li, W.Z. Zhang, Q.C. Wang, Y. An, Y.H. Li, Dynamic wavelength characteristics of semiconductor laser in electric current tuning process. Spectros. Spectr. Anal. **35**(11), 3220–3223 (2015)
22. J.W. Liu, Z.H. Du, J.Y. Li, R.B. Qi, K.X. Xu, Analytical model for the tuning characteristics of static, dynamic, and transient behaviors in temperature and injection current of DFB laser diodes. Acta Phys. Sin. **60**(7), 074213 (2011)
23. A. Lytkine, W. Jäger, J. Tulip, Frequency tuning of long-wavelength VCSELs. Spectrochim. Acta A **63**, 940–946 (2006)
24. S. Schilt, L. Thévenaz, Experimental method based on wavelength-modulation spectroscopy for the characterization of semiconductor lasers under direct modulation. Appl. Opt. **43**(22), 4446–4453 (2004)
25. J. Chen, A. Hangauer, R. Strzoda, M.C. Amann, Accurate extraction method for the FM response of tunable diode lasers based on wavelength modulation spectroscopy. Appl. Phys. B **90**, 243–247 (2008)
26. A. Hangauer, J. Chen, R. Strzoda, M.C. Amann, The frequency modulation response of vertical-cavity surface-emitting lasers: experiment and theory. IEEE J. Sel. Top. Quantum Electron. **17**(6), 1584–1593 (2011)
27. J.Y. Li, Z.H. Du, Y. An, Frequency modulation characteristics for interband cascade lasers emitting at 3 μm. Appl. Phys. B **121**(1), 7–17 (2015)